Spin density and spin torque induced by the D'yakonov-Perel' mechanism in magnetic semiconductor nanowires with a constriction

V. Fallahi*

Department of Laser and Optical Engineering, University of Bonab, Bonab 5551761167, Iran

(Received 13 August 2018; revised manuscript received 1 November 2018; published 8 January 2019)

The transport through a domain wall pinned at a nanoconstriction in (Ga,Mn)As wires is investigated theoretically using the Landauer-Büttiker approach by considering the Rashba and Dresselhaus spin-orbit interactions. The local nonequilibrium spin densities produced by electrical spin injection at the nanoconstriction are calculated numerically along the nanowire. The adiabatic and nonadiabatic components of the spin-transfer torque, expressed in terms of the gradient of the spin current density, are also computed. An oscillatory behavior in the spin-transfer torque is observed for the systems containing atomically sharp domain walls, due to the strong reflections at the domain wall caused by the large magnetization gradient. It is demonstrated that the strength of the oscillations for nonadiabatic spin torque increases by the negative Rashba parameter α_x, while it decreases with increasing positive values of α_x. However, the nonadiabatic spin torque increases with $|\alpha_y|$, regardless of its sign. Furthermore, it is shown that the Dresselhaus coupling β does not considerably alter the z component of the spin torque, while the other two components are effectively changed by the Dresselhaus spin-orbit interaction.

DOI: 10.1103/PhysRevB.99.024408

I. INTRODUCTION

Investigation of the interaction between spin-polarized electric currents and locally inhomogeneous magnetic textures of the domain walls has recently attracted much attention from both fundamental and technological viewpoints. Controlled manipulation of the domain wall configuration by spin-polarized currents is an important issue for its potential applications in spintronic devices such as logic gates [1], shift registers [2,3] as the basic building blocks of magnetic racetrack memories [4], and nonvolatile magnetic random access memories [5,6], whose functionalities are based on the domain wall motion through the spin-transfer torque effect. Thus a detailed understanding of the domain wall interaction with spin-polarized current is essential to explore new functionalities in spintronics.

Since the prediction of the current-induced spin-transfer torque phenomenon by Slonczewski [7] and Berger [8], different formalisms have been proposed to treat the interaction between the local magnetic moments and spin-polarized currents either in the ballistic [9,10] or diffusive regime [11–14]. For a thick domain wall of width d, the magnetization rotation frequency in terms of the electron Fermi velocity $\omega_{\text{Wall}} = \pi v_F/d$ is negligible compared to the pseudo-Larmor frequency of the spin, which is determined by the s-d exchange interaction energy Δ_{ex} as $\omega_{sd} = \Delta_{\text{ex}}/\hbar$; so, the polarization axis of the carriers can follow the local magnetic moments adiabatically, and thus the diffusive regime is expected to prevail. In the complete adiabatic limit, the dominant contribution to the spin-transfer torque is due to the loss of the spin angular momentum of the carriers passing through the domain wall. This so-called adiabatic spin-transfer torque is a reactive torque that tends to twist the magnetization of the domain wall. It preserves the time-reversal symmetry and is proportional to $-(\boldsymbol{j}\cdot\nabla)\boldsymbol{u}_M(r)$, where $\boldsymbol{u}_M(r)$ is the unit vector along the magnetization direction and $\boldsymbol{j}$ stands for the charge current density vector. For domain walls of intermediate widths, the mistracking between the carriers spin and the local magnetization leads to a nonadiabatic spin torque normal to the adiabatic term and proportional to $-\boldsymbol{u}_M\times(\boldsymbol{j}\cdot\nabla)\boldsymbol{u}_M(r)$. Such a torque is not invariant under the time reversal transformation ($\boldsymbol{u}_M \longrightarrow -\boldsymbol{u}_M$) and thus contributes to a dissipative process. Although the nonadiabatic spin torque strength is two orders of magnitude smaller than that of adiabatic term in the wide domain walls, it determines the critical current density needed to drive domain wall motion in zero magnetic field. Furthermore, the nonadiabatic torque produces a pressure directly on the domain wall when applying a dc current, while it contributes to the wall motion in the ac current case [15,16]. On the other hand, in the limit of narrow domain walls ($d \ll k_F^{-1}$), the adiabaticity does not take place and a strong reflection at the domain wall position may occur. Surprisingly, an atomic-scale domain wall, constructed by pulling off two antiparallel-aligned ferromagnetic electrodes in contact [17–20] or fabricated by electrodeposition techniques [21–23], shows an extremely huge magnetoresistance [24–29] commonly known as ballistic magnetoresistance (BMR). This may account for a significant enhancement of local spin accumulation [30] and thus an increase in both adiabatic and nonadiabatic spin torques [31]. The spin-transfer torque observed in ballistic domain walls can be understood in terms of the electron's scattering by geometrical domain wall potential. Fully nonadiabatic scattering of the carriers by the large induced magnetization gradient within the sharp domain walls leads to a relatively large nonadiabatic torque which results in the current-driven domain wall motion at low current densities [32,33]. This improves the efficiency of the

*v.fallahi@bonabu.ac.ir

spin-transfer torque effect and provides a route towards low power magnetic devices.

Another mechanism to influence the current-induced spin-transfer torque is based on the spin-orbit interactions caused by the D'yakonov-Perel' mechanism. The D'yakonov-Perel' spin relaxation in both metals and semiconductors, resulting from the lack of inversion symmetry, is expected to affect the current-induced spin torque through an increase in the spin-flip rate. This mechanism typically dominates the spin dynamics in p- (as well as in n-) doped samples, like the situation in (Ga,Mn)As semiconductors with relatively low hole densities [34–36]. The D'yakonov-Perel' spin scattering is derived by two momentum-dependent magnetic fields due to the bulk inversion asymmetry (Dresselhaus field) and structure inversion asymmetry (Rashba field). It is expected that in low-dimensional semiconductor structures, the nonadiabatic spin torque is considerably affected by the spin-orbit couplings. Through the calculations based on the standard Kohn-Luttinger Hamiltonian for a zinc-blende magnetic semiconductor, it has been shown that the spin-orbit interaction strongly enhances the current-induced nonadiabatic torque and thereby the domain wall velocity [37]. In an analogous theoretical approach, Yuan and Kelly [38] demonstrated the incremental contribution of the spin-orbit coupling to the nonadiabatic spin-transfer torque parameter of clean Ni domain walls. Similar results were obtained by Obata and Tatara [39], who considered the transport properties, in the presence of Rashba interaction, through the analysis of an effective Hamiltonian within the framework of Keldysh Green's function formalism. The critical current density required to initiate domain wall motion in a ferromagnetic semiconductor was predicted to be about three to four orders of magnitude smaller than that in a non-spin-orbit coupled system. Subsequently, a simple physical picture was proposed by Manchon and Zhang [40] to describe the combined effect of spin-orbit coupling and exchange interaction using the Boltzmann formulation. Focusing on the first-order terms of Rashba and Dresselhaus spin-orbit coupling parameters, they theoretically predicted that the spin-orbit torque can be effectively used to switch the magnetization direction, utilizing critical current densities as low as 10^4–10^6 A/cm^2 in a single ferromagnetic layer. The investigation was followed in Ref. [41], where Li *et al.* found a strong correlation between the angular dependence of the torque and the anisotropy of the Fermi surface. In both works, they considered a uniformly magnetized single layer, without any noncollinearity of the magnetization. In such a system, the homogeneous current-induced spin polarization provides a uniform torque on the collinear magnetization. Comparable results would be found in a noncollinear structure with low magnetization gradient, e.g., in a long domain wall, where the adiabatic (or in-plane) spin-transfer torque remains relatively constant in each segment of the whole structure. In this case, the adiabatic spin-transfer torque would translate the noncollinear magnetic texture without any distortion. On the other hand, the emergence of a nonuniform spin torque in a noncollinear structure with large magnetization gradient would distort the magnetization profile. More especially, the distortion seems to be significantly affected by the spin-orbit torque induced by the Rashba and Dresselhaus effects in a diluted magnetic semiconductor, which to my knowledge has not been addressed in the literature. Here, I assume a finite-sized ballistic domain wall between two ferromagnetic regions and study the effect of the Rashba and Dresselhaus spin-orbit couplings on the spin polarization and spin-transfer torque in the ballistic transport regime. The outline of the remainder of this paper is as follows.

In Sec. II, I discuss the general algorithm used to solve the coupled spin channels Schrödinger equation with mixed Dirichlet-Neumann boundary conditions in details. The approach presented in this section, can be utilized for domain walls with complex magnetic textures. Also, the spin-dependent transport properties of a ballistic domain wall pinned at a semiconducting magnetic nanocontact, such as conductance, nonequilibrium spin density and spin-orbit torque, are explored. In Sec. III, the quantum conductance of carriers is calculated for an atomic-scale domain wall in the presence of the Rashba and Dresselhaus spin-orbit couplings. The accumulated spin density within the wall and its surroundings is computed and then the resulting spin-transfer torque exerted on the local magnetization is quantified. The effect of the spin-orbit couplings on the spin density and spin-transfer torque components are also discussed. Finally, a brief summary and conclusions will be provided in Sec. IV.

II. THEORETICAL CONSIDERATIONS

I consider a p-type semiconducting ferromagnetic nanowire containing a head-to-head domain wall of width d. The thickness of the nanowire (a few monolayers) is selected in such a way that just one transverse channel participates in the transport. In such an ultrathin nanowire, Néel-type domain walls would be more favorable below a critical wire thickness (less than the wall width d), while the Bloch walls would be found in the bulk materials. The magnetization profile in the walls formed in nanocontacts has been mostly described by a simple tanh profile in the theoretical literatures [42–44].

As illustrated in Fig. 1, the local magnetic moments orientation in the domain wall plane is well described by the function $\theta(z) = \cos^{-1}[-\tanh(\frac{\pi^2 z}{2d})]$, for $-\infty \leqslant z \leqslant \infty$. The single-hole Hamiltonian of the system in the presence of the Rashba and Dresselhaus spin-orbit couplings, utilizing an

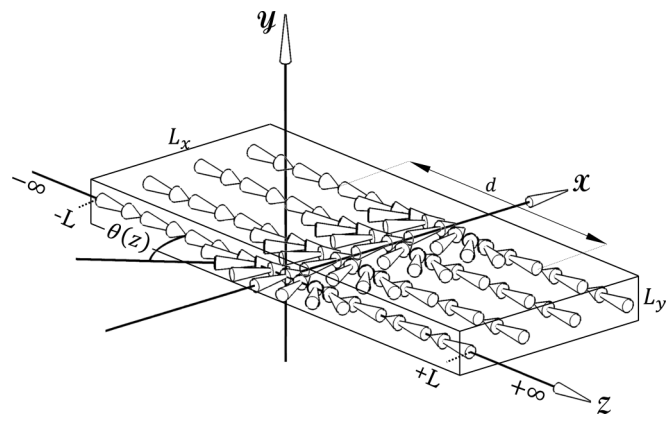

FIG. 1. Sketch of a head-to-head domain wall pinned at a nanocontact between two p-type semiconducting magnetic nanowires.

effective one-band model approach, can be written as

$$H = \frac{p^2}{2m^*} + V_\perp(x, y) - \frac{\Delta_{\rm ex}}{2}\hat{\boldsymbol{\sigma}} \cdot \boldsymbol{u}_M(z) + H_R + H_D, \quad (1)$$

where $\Delta_{\rm ex}$ is the spin splitting energy, $V_\perp(x, y)$ represents the confinement potential, $\hat{\boldsymbol{\sigma}}$ denotes the spin operators in terms of the Pauli spin matrices, and $\boldsymbol{u}_M(z) = [\sin\theta(z), 0, \cos\theta(z)]$ indicates the unit vector parallel to the local magnetization. H_R and H_D are the Rashba and Dresselhaus Hamiltonians, respectively. The confinement potential can be considered as

$$V_\perp(x, y) = U(x) + U(y) + V_g(x, y), \quad (2)$$

in which $U(x)$ and $U(y)$ are the confining potentials arising from the dimensional constraints in the lateral directions which define the transverse modes in the system. The potential $V_g(x, y)$ attributes to the lateral gates in the system that alters the strength of the lateral confining potential. The confinement potential in the lateral dimensions offers the possibility of defining a quasi-one-dimensional Hamiltonian. On the other hand, the nanometric cross-sectional dimensions of the nanowire are small enough compared to the Fermi wavelength of the carriers; so, only a single transverse channel participates in the transport, a situation typically achieved in low-dimensional magnetic semiconductors. Therefore one can introduce one-dimensional Hamiltonians for the Rashba and Dresselhaus spin-orbit terms by averaging of the transverse momenta over the ground-state eigenfunction of the confinement potential.

In general, there is a major difference between the Rashba spin splitting terms in the hole systems and the more familiar electron gas systems. However, the effective Rashba Hamiltonian for the light-hole states is the same as the corresponding Hamiltonian for the electron states in the Γ_6^c conduction band [45]:

$$H_e^{6c} = \gamma_R \boldsymbol{k} \times \boldsymbol{E} \cdot \boldsymbol{\sigma}, \quad (3)$$

in which γ_R is the strength of the Rashba spin-orbit interaction, $\boldsymbol{k}$ refers to the wave vector and $\boldsymbol{E}$ is the electric field that characterizes the spatial inversion asymmetry of the confining potential. As can be seen, H_e^{6c} is linear in $\boldsymbol{k}$, while there is a cubic dependence of the spin splitting term on the in-plane wave vector in the Γ_8^v valence band for the heavy-hole states in two-dimensional hole systems. However, in the theoretical work performed by Kernreiter *et al.* [46], it has been suggested that when the holes are confined in the quasi-one-dimensional systems, the Rashba term once again becomes linear in $\boldsymbol{k}$ term. Then, the effective magnetic field vector induced by the Rashba term always lies perpendicular to the one-dimensional channel, similar to the electron case.

So, the Rashba spin-orbit interaction can be stated as

$$\begin{aligned} H_R = \frac{\gamma_R}{\hbar}\{&\sigma_x(\langle\partial_y V_\perp\rangle p_z - \langle\partial_z V_\perp\rangle\langle p_y\rangle) \\ &+ \sigma_y(\langle\partial_z V_\perp\rangle\langle p_x\rangle - \langle\partial_x V_\perp\rangle p_z) \\ &+ \sigma_z(\langle\partial_x V_\perp\rangle\langle p_y\rangle - \langle\partial_y V_\perp\rangle\langle p_x\rangle)\}. \end{aligned} \quad (4)$$

Since the carriers transport along the z axis, one should consider p_z in the Hamiltonian as an operator, $-i\hbar\partial/\partial z$. Denoting the cross-sectional dimensions of the nanowire by L_x and L_y, one can obtain: $\langle p_x\rangle = 0$, $\langle p_y\rangle = 0$, $\langle p_x^2\rangle = \hbar^2\pi^2/L_x^2$, and $\langle p_y^2\rangle = \hbar^2\pi^2/L_y^2$. Therefore H_R can be rewritten as

$$H_R = -i(\alpha_y\sigma_x - \alpha_x\sigma_y)\frac{\partial}{\partial z}, \quad (5)$$

where $\alpha_q = \gamma_R\langle\partial_q V_\perp\rangle$, $(q = x, y)$ is the Rashba coupling constant. It has been shown that the average values of $\langle\partial_q V_\perp\rangle$ are of the order of a few meV/Å [47]. Taking into account the values of γ_R for different semiconductors, the value of α_q can vary in the range of a few meVnm to a few tens meVnm in low-dimensional systems [47–49]. As pointed, the Rashba spin-orbit coupling term arises from the lateral confining potentials and its strength can be modified by applying an additional field via lateral gates. Moreover, both negative and positive values are possible for the Rashba spin-orbit constant, depending on the direction of the applied field.

The Dresselhaus spin-orbit interaction can be controlled by choosing the crystallographic growth direction in which the sample is fabricated. Moreover, the strain-induced spin-orbit coupling of the Dresselhaus type would be found, when a p-type ferromagnetic semiconductor with zinc-blende crystal structure is subjected to strain [50,51]. One can therefore assume a linear dependence on the wave vector in the case of Dresselhaus spin-orbit coupling, in order to consider the effective magnetic field vector parallel to the transport direction:

$$H_D = -i\beta\sigma_z\frac{\partial}{\partial z}, \quad (6)$$

where β denotes the Dresselhaus coupling constant. The real III-V magnetic semiconductors like (Ga,Mn)As are known to have rather complex band structures consisting of several hole subbands with the spin-orbit interactions included in the hole Hamiltonian. The effective one-band model with parabolic subbands is only valid for energies much less than the energy of the spin-orbit splitting Δ_{SO}. However, in a general case, the theory of hole transport in p-(Ga,Mn)As needs special consideration.

The coupled Schrödinger equations for "up" and "down" components of the wave function ($\Phi^{\uparrow(\downarrow)}$) are then

$$\begin{aligned} &\left[\frac{d^2}{dz^2} + k_F^2 - k_{\rm ex}^2\tanh\left(\frac{\pi^2 z}{2d}\right)\right]\Phi^\uparrow(z) - 2ik_D\frac{d}{dz}\Phi^\uparrow(z) \\ &\quad + k_{\rm ex}^2{\rm sech}\left(\frac{\pi^2 z}{2d}\right)\Phi^\downarrow(z) - 2k_R e^{-i\varphi_R}\frac{d}{dz}\Phi^\downarrow(z) = 0 \end{aligned} \quad (7a)$$

and

$$\begin{aligned} &\left[\frac{d^2}{dz^2} + k_F^2 + k_{\rm ex}^2\tanh\left(\frac{\pi^2 z}{2d}\right)\right]\Phi^\downarrow(z) + 2ik_D\frac{d}{dz}\Phi^\downarrow(z) \\ &\quad + k_{\rm ex}^2{\rm sech}\left(\frac{\pi^2 z}{2d}\right)\Phi^\uparrow(z) + 2k_R e^{+i\varphi_R}\frac{d}{dz}\Phi^\uparrow(z) = 0, \end{aligned} \quad (7b)$$

in which $k_F = \sqrt{\frac{2m^*\epsilon_F}{\hbar^2}}$ is the Fermi wave vector, and the exchange coupling term is described by the wave vector $k_{\rm ex} = \sqrt{\frac{m^*\Delta_{\rm ex}}{\hbar^2}}$. The strengths of the Rashba and Dresselhaus spin-orbit couplings are measured in terms of the characteristic wave vectors $k_R = \frac{m^*\alpha_R}{\hbar^2}$ and $k_D = \frac{m^*\beta}{\hbar^2}$, respectively, where $\alpha_R = \sqrt{\alpha_x^2 + \alpha_y^2}$ is the Rashba spin-orbit coupling strength,

and $\varphi_R = \tan^{-1}\frac{\alpha_y}{\alpha_x}$ represents the direction of the Rashba field.

These coupled spin channels Schrödinger equations can be solved numerically using an appropriate finite difference scheme and utilizing boundary conditions defined at the boundaries [52]. However, the boundary conditions in the aforementioned problem that contains the central scattering region (domain wall) and two semi-infinite left and right leads, are not clearly defined; they depend on the unknown values of reflection ($r^{\uparrow(\downarrow)}$) and transmission ($t^{\uparrow(\downarrow)}$) amplitudes that would be obtained, later. In the proposed algorithm, which is applicable to both adiabatic and nonadiabatic transport regimes, first, the mixed boundary conditions in the left and right leads, far away from the domain wall, are found by eliminating the reflection and transmission amplitudes, and then the coupled Schrödinger equations are solved using a finite difference method based on the three-stage Lobatto IIIa implicit Runge-Kutta formula. According to Fig. 1, that shows a noncollinear magnetic structure between two uniformly magnetized leads, the whole structure including the domain wall and ferromagnetic leads is divided into N segments along the z axis in a way that the direction of magnetization remains approximately constant in each segment.

The full wave function of an incident (reflected) carrier in the left side ($\mathcal{L}$) and transmitted carrier to the right side ($\mathcal{R}$) with the Fermi energy ϵ_F may be written as

$$\Phi = \frac{e^{\pm ik_{i(r)(t)}z}}{\sqrt{|A_{i(r)(t)}|^2 + |B_{i(r)(t)}|^2}}\begin{pmatrix} A_{i(r)(t)} \\ B_{i(r)(t)} \end{pmatrix}, \tag{8}$$

in which $k_{i(r)(t)}$ represents the longitudinal wave vector of the spin states at the Fermi surface (the subscripts i, r, and t refer to the incident, reflected, and transmitted waves, respectively). In order to find the wave vectors of the incident ($k_i^{\uparrow(\downarrow)}$) and reflected (transmitted) ($k_{r(t)}^{\uparrow(\downarrow)}$) spin states, the determinant of the matrix $|H - \epsilon_F I|$ must be set to zero:

$$\left(k^2 - k_F^2\right)^2 - \left(k_{\rm ex}^2 \mp 2kk_D\right)^2 - 4k^2k_R^2 = 0. \tag{9}$$

By substituting the wave vectors $k_{i(r)}^{\uparrow(\downarrow)}$ in the characteristic equation of the matrix H, I can find the spin function coefficients $A_{i(r)(t)}$ and $B_{i(r)(t)}$ for both up- and down-spin states:

$$|\uparrow\rangle_{i(r)(t)} = \frac{\begin{bmatrix} 1 \\ -\tan\frac{\theta_{i(r)(t)}}{2}e^{i\phi_{i(r)(t)}} \end{bmatrix}}{\sqrt{1 + \tan\frac{\theta_{i(r)(t)}}{2}\tan\frac{\theta^*_{i(r)(t)}}{2}}}, \tag{10a}$$

$$|\downarrow\rangle_{i(r)(t)} = \frac{\begin{bmatrix} \tan\frac{\theta^*_{i(r)(t)}}{2}e^{-i\phi_{i(r)(t)}} \\ 1 \end{bmatrix}}{\sqrt{1 + \tan\frac{\theta_{i(r)(t)}}{2}\tan\frac{\theta^*_{i(r)(t)}}{2}}}, \tag{10b}$$

in which

$$\theta_{i(r)}^{\uparrow(\downarrow)} = 2\tan^{-1}\frac{\pm\frac{2k_{i(r)}^{\uparrow(\downarrow)}k_R}{k_{\rm ex}^2 \mp 2k_{i(r)}^{\uparrow(\downarrow)}k_D}}{1 + \sqrt{1 + \left(\frac{2k_{i(r)}^{\uparrow(\downarrow)}k_R}{k_{\rm ex}^2 \mp 2k_{i(r)}^{\uparrow(\downarrow)}k_D}\right)^2}}, \tag{11a}$$

$$\theta_t^{\uparrow(\downarrow)} = 2\pi - 2\tan^{-1}\frac{\frac{2k_t^{\uparrow(\downarrow)}k_R}{k_{\rm ex}^2 + 2k_t^{\uparrow(\downarrow)}k_D}}{1 + \sqrt{1 + \left(\frac{2k_t^{\uparrow(\downarrow)}k_R}{k_{\rm ex}^2 + 2k_t^{\uparrow(\downarrow)}k_D}\right)^2}}, \tag{11b}$$

and $\phi_{i(r)(t)} = \varphi_R - \frac{\pi}{2}$ defines the direction of the spin quantization axis in spherical coordinates (θ , ϕ) for incident, reflected, and transmitted spin states. Then, I can write the wave functions on both sides of the nanocontact as

$$\Psi_{k,\mathcal{L}}(z) = I^{\uparrow}\begin{pmatrix} A_i^{\uparrow} \\ B_i^{\uparrow} \end{pmatrix}e^{ik_i^{\uparrow}z} + r^{\uparrow}\begin{pmatrix} A_r^{\uparrow} \\ B_r^{\uparrow} \end{pmatrix}e^{-ik_r^{\uparrow}z} + I^{\downarrow}\begin{pmatrix} A_i^{\downarrow} \\ B_i^{\downarrow} \end{pmatrix}e^{ik_i^{\downarrow}z} + r^{\downarrow}\begin{pmatrix} A_r^{\downarrow} \\ B_r^{\downarrow} \end{pmatrix}e^{-ik_r^{\downarrow}z} \tag{12a}$$

and

$$\Psi_{k,\mathcal{R}}(z) = t^{\uparrow}\begin{pmatrix} A_t^{\uparrow} \\ B_t^{\uparrow} \end{pmatrix}e^{ik_t^{\uparrow}z} + t^{\downarrow}\begin{pmatrix} A_t^{\downarrow} \\ B_t^{\downarrow} \end{pmatrix}e^{ik_t^{\downarrow}z}, \tag{12b}$$

where $I^{\uparrow(\downarrow)}$ are the incoming "up" and "down" spin wave intensities. The scattering states $\Psi_{k,\mathcal{L}}(z)$ and $\Psi_{k,\mathcal{R}}(z)$ describe the incoming spin waves from $z = -\infty$ to the right, which are partially reflected and partially transmitted into the two spin channels. The coefficients $t^{\uparrow(\downarrow)}$ and $r^{\uparrow(\downarrow)}$ are the transmission and reflection amplitudes, respectively. In order to calculate the transmission amplitudes, I first assume the incoming wave to be entirely "up" and then consider purely "down" spin state. The full wave function in the scattering and its surrounding regions can be obtained numerically by solving the second-order differential equations that satisfy the following boundary conditions at $z = \pm L$, sufficiently far from the scattering region:

$$\begin{vmatrix} ik_i^{\uparrow}A_i^{\uparrow} & -ik_r^{\uparrow}A_r^{\uparrow} & -ik_r^{\downarrow}A_r^{\downarrow} \\ A_i^{\uparrow} & A_r^{\uparrow} & A_r^{\downarrow} \\ B_i^{\uparrow} & B_r^{\uparrow} & B_r^{\downarrow} \end{vmatrix} I^{\uparrow}e^{-ik_i^{\uparrow}L} + \begin{vmatrix} ik_i^{\downarrow}A_i^{\downarrow} & -ik_r^{\uparrow}A_r^{\uparrow} & -ik_r^{\downarrow}A_r^{\downarrow} \\ A_i^{\downarrow} & A_r^{\uparrow} & A_r^{\downarrow} \\ B_i^{\downarrow} & B_r^{\uparrow} & B_r^{\downarrow} \end{vmatrix} I^{\downarrow}e^{-ik_i^{\downarrow}L} = \begin{vmatrix} \Phi'^{\uparrow}(1) & -ik_r^{\uparrow}A_r^{\uparrow} & -ik_r^{\downarrow}A_r^{\downarrow} \\ \Phi^{\uparrow}(1) & A_r^{\uparrow} & A_r^{\downarrow} \\ \Phi^{\downarrow}(1) & B_r^{\uparrow} & B_r^{\downarrow} \end{vmatrix}, \tag{13a}$$

$$\begin{vmatrix} ik_i^{\uparrow}B_i^{\uparrow} & -ik_r^{\uparrow}B_r^{\uparrow} & -ik_r^{\downarrow}B_r^{\downarrow} \\ A_i^{\uparrow} & A_r^{\uparrow} & A_r^{\downarrow} \\ B_i^{\uparrow} & B_r^{\uparrow} & B_r^{\downarrow} \end{vmatrix} I^{\uparrow}e^{-ik_i^{\uparrow}L} + \begin{vmatrix} ik_i^{\downarrow}B_i^{\downarrow} & -ik_r^{\uparrow}B_r^{\uparrow} & -ik_r^{\downarrow}B_r^{\downarrow} \\ A_i^{\downarrow} & A_r^{\uparrow} & A_r^{\downarrow} \\ B_i^{\downarrow} & B_r^{\uparrow} & B_r^{\downarrow} \end{vmatrix} I^{\downarrow}e^{-ik_i^{\downarrow}L} = \begin{vmatrix} \Phi'^{\downarrow}(1) & -ik_r^{\uparrow}B_r^{\uparrow} & -ik_r^{\downarrow}B_r^{\downarrow} \\ \Phi^{\uparrow}(1) & A_r^{\uparrow} & A_r^{\downarrow} \\ \Phi^{\downarrow}(1) & B_r^{\uparrow} & B_r^{\downarrow} \end{vmatrix}, \tag{13b}$$

$$\begin{vmatrix} \Phi'^{\uparrow}(N) & ik_t^{\uparrow}A_t^{\uparrow} & ik_t^{\downarrow}A_t^{\downarrow} \\ \Phi^{\uparrow}(N) & A_t^{\uparrow} & A_t^{\downarrow} \\ \Phi^{\downarrow}(N) & B_t^{\uparrow} & B_t^{\downarrow} \end{vmatrix} = 0, \tag{13c}$$

$$\begin{vmatrix} \Phi'^{\downarrow}(N) & ik_t^{\uparrow}B_t^{\uparrow} & ik_t^{\downarrow}B_t^{\downarrow} \\ \Phi^{\uparrow}(N) & A_t^{\uparrow} & A_t^{\downarrow} \\ \Phi^{\downarrow}(N) & B_t^{\uparrow} & B_t^{\downarrow} \end{vmatrix} = 0, \tag{13d}$$

in which $\Phi'^{\uparrow(\downarrow)}$ indicate the derivatives of the two-component spinor wave function. The aforementioned mixed boundary conditions in the left and right leads are obtained by eliminating the unknown reflection and transmission amplitudes in the continuity relations of the wave function and its derivative. Subsequently, the reflection and transmission coefficients will be obtained as follows:

$$t^{\uparrow(\downarrow)} = \pm\frac{B_t^{\downarrow(\uparrow)}\Phi^{\uparrow}(N) - A_t^{\downarrow(\uparrow)}\Phi^{\downarrow}(N)}{A_t^{\uparrow}B_t^{\downarrow} - A_t^{\downarrow}B_t^{\uparrow}}e^{-ik_i^{\uparrow(\downarrow)}L}, \tag{14}$$

$$r^{\uparrow(\downarrow)} = \pm\frac{\begin{vmatrix} A_r^{\downarrow(\uparrow)} & A_i^{\uparrow}I^{\uparrow}e^{-ik_i^{\uparrow}L} + A_i^{\downarrow}I^{\downarrow}e^{-ik_i^{\downarrow}L} - \Phi^{\uparrow}(1) \\ B_r^{\downarrow(\uparrow)} & B_i^{\uparrow}I^{\uparrow}e^{-ik_i^{\uparrow}L} + B_i^{\downarrow}I^{\downarrow}e^{-ik_i^{\downarrow}L} - \Phi^{\downarrow}(1) \end{vmatrix}}{(A_r^{\uparrow}B_r^{\downarrow} - A_r^{\downarrow}B_r^{\uparrow})e^{ik_r^{\uparrow(\downarrow)}L}}. \tag{15}$$

I use the two-probe Landauer formula to obtain the conductivity from the transmission coefficients. The transmission coefficients are evaluated as the ratio of the transmitted to the incident probability current density as follows:

$$T^{pq} = \frac{k_t^q|t^q|^2}{k_i^p|I^p|^2}\Xi\left(k_i^p\right)\Xi\left(k_t^q\right), \quad p,q = \uparrow \text{ and } \downarrow. \tag{16}$$

Then, the total transmission coefficients for the incoming up- and down-spin states will be equal to $T^{\uparrow} = T^{\uparrow\uparrow} + T^{\uparrow\downarrow}$ and $T^{\downarrow} = T^{\downarrow\uparrow} + T^{\downarrow\downarrow}$, respectively. The Heaviside function $\Xi(k)$ is considered in order to eliminate evanescent spin wave functions. In this way, $\Xi(k)$ will be equal to zero in the case of $\mathrm{Im(k)} \neq 0$.

Assuming that the incoming electronic spin is an unpolarized statistical mixture, i.e., $\rho_{in} = \frac{1}{2}(|\uparrow\rangle\langle\uparrow| + |\downarrow\rangle\langle\downarrow|)$, the output will be obtained by $\rho_{\text{out}} = \frac{1}{2}[(T^{\uparrow\downarrow} + T^{\downarrow\downarrow})|\uparrow\rangle\langle\uparrow| + (T^{\downarrow\uparrow} + T^{\uparrow\uparrow})|\downarrow\rangle\langle\downarrow|]$ [53]. Therefore the overall transmission coefficient of the unpolarized electrons will be given by $T = \frac{1}{2}(T^{\uparrow} + T^{\downarrow})$. In the case reported here, the possibility that electrons could be partially polarized before ballistic transport through the ferromagnetic material is not take into account.

At low bias voltage, the domain wall conductance is calculated according to the Landauer-Büttiker formalism [54]. This approach, which is widely used in mesoscopic physics, expresses the conductance in terms of the transmission properties of coherent electron states as follows:

$$\mathcal{G} = \frac{2e^2}{h}T. \tag{17}$$

The nonequilibrium spin density (spin accumulation) produced in the domain wall with inhomogeneous magnetic texture can exert a torque on the domain wall and the neighboring ferromagnetic contacts. In the limit of infinitesimal bias voltage applied across the domain wall, $e\delta V = \mu_{\mathcal{L}} - \mu_{\mathcal{R}}$, I considered both right-going "up" spin holes from the left lead and left-going "down" spin holes from the right lead at the chemical potentials $\mu_{\mathcal{L}} = \epsilon_F + \frac{e\delta V}{2}$ and $\mu_{\mathcal{R}} = \epsilon_F - \frac{e\delta V}{2}$, respectively. For the process to be possible, the majority spin holes must be available at the chemical potential $\mu_{\mathcal{L}(\nabla)}$ in the left (right) lead $[f_{\mathcal{L}(\nabla)}(\epsilon)]$, while the right (left) lead must be unoccupied $[1 - f_{\mathcal{R}(\mathcal{L})}(\epsilon)]$. Functions $f_{\mathcal{L}(\nabla)} = [\exp(\frac{\epsilon - \mu_{\mathcal{L}(r)}}{k_B T}) + 1]^{-1}$ are Fermi-Dirac distributions in the left and right lead at temperature T, respectively. Based on the single-electron model, the nonequilibrium spin density of the system could be estimated by integrating over the entire energy as follows:

$$\langle \boldsymbol{m}\rangle^{ne} = \frac{1}{e\delta V}\int_{-\infty}^{+\infty} d\epsilon[\overset{\mathcal{L}\to\mathcal{R}}{\langle \boldsymbol{m}\rangle} f_{\mathcal{L}}(\epsilon)(1 - f_{\mathcal{R}}(\epsilon)) - \overset{\mathcal{R}\to\mathcal{L}}{\langle \boldsymbol{m}\rangle} f_{\mathcal{R}}(\epsilon)(1 - f_{\mathcal{L}}(\epsilon))], \tag{18}$$

where $\boldsymbol{m} = \mu_B\boldsymbol{\sigma}$ represents the magnetization of the carriers, and μ_B is the Bohr magneton. The Fermi distribution function is expanded around the point $(\epsilon - \epsilon_F)$ as $f_{\mathcal{L}(\nabla)}(\epsilon) = \Theta(\epsilon_F - \epsilon) \mp \frac{e\delta V}{2}\delta(\epsilon - \epsilon_F)$ in the limit of absolute zero temperature to derive the above equation [55]. This equation is analogous to Eq. (14) in Ref. [38] for right-going electrons from the left lead and left-going holes from the right lead. The spatial profile of the transverse ($x - y$ plane) and longitudinal (z-axis) components of the spin accumulation would be calculated numerically as follows:

$$\langle \boldsymbol{m}(z)\rangle^{ne} = \frac{\overset{\mathcal{L}\to\mathcal{R}}{\langle \boldsymbol{m}(z)\rangle} + \overset{\mathcal{R}\to\mathcal{L}}{\langle \boldsymbol{m}(z)\rangle}}{2}. \tag{19}$$

The total spin accumulation density induced by the external current $I_0 = \frac{e^2\delta V}{\pi\hbar}T$, can be obtained as the integral of the spin density over all energies between $\epsilon_F - \frac{e\delta V}{2}$ and $\epsilon_F + \frac{e\delta V}{2}$:

$$\langle \boldsymbol{m}\rangle^{ne}_{\text{tot}} = e\delta V\mathcal{N}(\epsilon_F)\langle \boldsymbol{m}\rangle^{ne} = \frac{3epI_0}{4\mathcal{G}\epsilon_F}\langle \boldsymbol{m}\rangle^{ne}, \tag{20}$$

in which $\mathcal{N}(\epsilon_F) = 3p/4\epsilon_F$ denotes the density of states in terms of the Fermi energy and p is the hole density.

It has been well known that the transverse components of the spin accumulation exert a torque on the magnetization of the domain wall. This torque would lead to the deformation of the wall and its surroundings on the scale of the Larmor precession length. The spin torque can be formulated in terms of the spin current density. The charge current density ($\boldsymbol{j}$) and the spin current density ($\overleftrightarrow{\mathcal{Q}}$) in the presence of the spin-orbit coupling can be defined by

$$\overset{\mathcal{L}\rightleftarrows\mathcal{R}}{\boldsymbol{j}} = \frac{e}{m^*}\mathrm{Re}\langle\psi|\overset{\mathcal{L}\rightleftarrows\mathcal{R}}{\boldsymbol{\pi}}|\psi\rangle, \tag{21}$$

$$\overset{\mathcal{L}\rightleftarrows\mathcal{R}}{\overleftrightarrow{\mathcal{Q}}} = \frac{\mu_B}{m^*}\mathrm{Re}\langle\psi|\boldsymbol{\sigma}\otimes\overset{\mathcal{L}\rightleftarrows\mathcal{R}}{\boldsymbol{\pi}}|\psi\rangle, \tag{22}$$

where $\overset{\mathcal{L}\rightleftarrows\mathcal{R}}{\pi}_{x(y)} = 0$ and $\overset{\mathcal{L}\rightleftarrows\mathcal{R}}{\pi}_z = \pm p_z \pm \frac{\alpha_y}{\hbar}\sigma_x \mp \frac{\alpha_x}{\hbar}\sigma_y \pm \frac{\beta}{\hbar}\sigma_z$ are three components of kinetic momentum operator which have odd symmetry under time reversal. The spin-orbit coupling

adds some extra terms to the canonical momentum p_z. Since the steady current flow is along the z axis, the tensor $\overleftrightarrow{\mathcal{Q}}$ can be considered as a vector with three components $\mathcal{Q}_{xz}$, $\mathcal{Q}_{yz}$, and $\mathcal{Q}_{zz}$ in spin-space coordinates. Similar to the spin accumulation, the charge current density and the three components of the spin current density would be calculated as follows:

$$\langle j_z(z)\rangle = \frac{\overset{\mathcal{L}\to\mathcal{R}}{\langle j_z(z)\rangle} + \overset{\mathcal{R}\to\mathcal{L}}{\langle j_z(z)\rangle}}{2}, \tag{23}$$

$$\langle \boldsymbol{\mathcal{Q}}(z)\rangle = \frac{\overset{\mathcal{L}\to\mathcal{R}}{\langle \boldsymbol{\mathcal{Q}}(z)\rangle} + \overset{\mathcal{R}\to\mathcal{L}}{\langle \boldsymbol{\mathcal{Q}}(z)\rangle}}{2}. \tag{24}$$

The total charge and spin current densities can be written as follows:

$$\langle j_z, \boldsymbol{\mathcal{Q}}\rangle_{\rm tot} = \frac{3epI_0}{4\mathcal{G}\epsilon_F}\langle j_z, \boldsymbol{\mathcal{Q}}\rangle. \tag{25}$$

The spin current is not conserved upon passing through the ferromagnetic structures with either collinear or noncollinear geometries. This is due to the possibility of reorientation of the carriers spin caused by the local exchange field in the ferromagnetic structures. However, the total angular momentum must be conserved as a result of Lorentz invariance. Thus the lost spin current must have been transferred to the local magnetic moments that acts as the so-called spin-transfer torque on the local magnetic moments. The net spin-transfer torque (per unit area) acting on the domain wall is then given by $\overleftrightarrow{\mathcal{N}}_{\rm STT,tot} = \overleftrightarrow{\mathcal{Q}}_{\rm tot}(z=-\frac{d}{2}) - \overleftrightarrow{\mathcal{Q}}_{\rm tot}(z=+\frac{d}{2})$, while the local spin-transfer torque per unit area (per unit distance) is calculated as $\overleftrightarrow{\mathcal{N}}_{\rm STT}(z) = -\frac{\partial}{\partial z}\overleftrightarrow{\mathcal{Q}}_{\rm tot}(z)$.

The spin-transfer torque can be decomposed into two parts: the adiabatic torque term which is proportional to $\boldsymbol{m}\times(\boldsymbol{m}\times\frac{\partial}{\partial z}\boldsymbol{m})$ (known as in-plane component that lies in the xz plane), and the nonadiabatic one which arises from the dissipation processes in spin dynamics [56], and is proportional to $\boldsymbol{m}\times\frac{\partial}{\partial z}\boldsymbol{m}$ (parallel to y axis, namely, out-of-plane component).

III. RESULTS AND DISCUSSION

The calculations have been performed for a 1-nm-thick domain wall residing in a nanoconstriction between two semiconducting magnetic nanowires with a constant spin splitting energy $\Delta_{\rm ex} = 0.5$ eV and valence hole effective mass $m^* = (m_{\rm HH}^{3/2} + m_{\rm LH}^{3/2})^{2/3} m_0 = 0.47\, m_0$, where $m_{\rm HH}$ and $m_{\rm LH}$ denote the heavy hole and light hole effective masses in units of the free electron mass m_0, respectively. The Fermi energy in a Mn-doped GaAs material has been considered to be $\epsilon_F = 0.2$ eV. The magnetic semiconductors with $\epsilon_F < \frac{\Delta_{\rm ex}}{2}$, referred to as half-metallic ferromagnets, can produce 100% spin polarization at the Fermi level. The spin relaxation length is typically of the order of tens of nanometers for the short spin relaxation time (≈0.1 ps) found in (Ga,Mn)As ferromagnetic semiconductors [57,58], which allows the spin-polarized carriers to preserve their spin orientation over a few nanometers, the length scale of the wall width. Therefore I considered the case in which the incident wave coming from the left (right) ferromagnetic lead is a pure spin-up (-down) state.

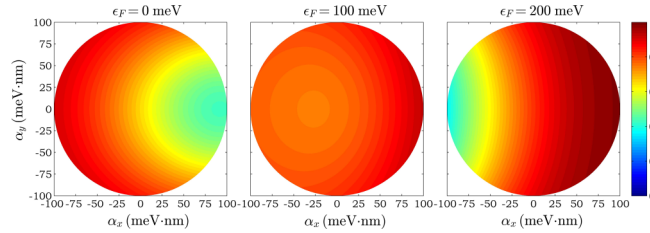

FIG. 2. The contour plot of the linear-response conductance (in the units of $\frac{e^2}{h}$) of a 1-nm-thick head-to-head domain wall in a (Ga,Mn)As nanowire with spin splitting energy $\Delta_{\rm ex} = 0.5$ eV, and Fermi energies (left) $\epsilon_F = 0.0$, (middle) 0.1, and (right) 0.2 eV as a function of the Rashba spin-orbit coupling parameter in the complex plane $\alpha_R e^{i\varphi_R}$, and in the case of $\beta = 0$.

In the linear response regime, the dependence of the domain wall conductance on the Fermi energy as a function of the complex Rashba parameter, $\alpha_R e^{i\varphi_R}$, has been shown in Fig. 2 for the symmetric lateral confinement potential $U(x) = U(y)$, where the Dresselhaus coupling constant is equal to zero. As can be seen, the conductance of a single-mode half-metallic ferromagnetic point contact is bounded by the upper limit $\frac{e^2}{h}$ (half of the expected limit of a one-dimensional perfect transmission channel), due to the spin blockade effect. It shows that the domain wall conductance increases (decreases) with the Fermi energy for positive (negative) α_x [59]. In contrast to the asymmetric behavior of the conductance as a function of α_x, a symmetric increase is observed in the wall conductance relative to the Rashba coupling strength $|\alpha_y|$, which is brought about by the transverse electric field $-\partial_y V_\perp$ along the y axis. Indeed, asymmetric spin precession around the magnetic field along the y axis, induced by the Rashba interaction (α_x), results in the asymmetry of the wall conductance. On the other hand, the symmetric behavior in the conductance is caused by the symmetric Rashba coupling parallel to the Néel-type domain wall plane. Increase (decrease) of the domain wall conductance as increasing the positive values (decreasing the negative values) of α_x can be explained in terms of the spin mistracking effect. In fact, the positive (negative) Rashba coupling α_x can be viewed as an effective magnetic field with the amplitude $\frac{2\hbar}{e}k_R k_i^{\uparrow}$ parallel (antiparallel) to the y axis for carriers coming from the left lead. This effective magnetic field makes the electrons spin precess counterclockwise (clockwise) about the y axis that facilitates (inhibits) the tracking between electron spin and the local magnetization direction $\boldsymbol{u}_M(z)$. The net effect is to increase (decrease) the domain wall conductance.

The asymmetry in the lateral confinement potential $U(x) \neq U(y)$ would introduce an additional linear Dresselhaus spin-orbit interaction in the quantum wire system. In homogeneous systems, there is no difference between the linear Dresselhaus interaction and the Rashba term, as they are related to each other by a unitary transformation. However, the Hamiltonian of the systems with noncollinear magnetization is not invariant under spin rotation and, thus, these spin-orbit couplings may result in different behaviors in the domain wall conductance. Figure 3 shows the conductance $\mathcal{G}(\alpha_R, \varphi_R, \beta)$ isosurface plots for a 1-nm-thick domain wall. The asymmetric (symmetric) behavior of the conductance

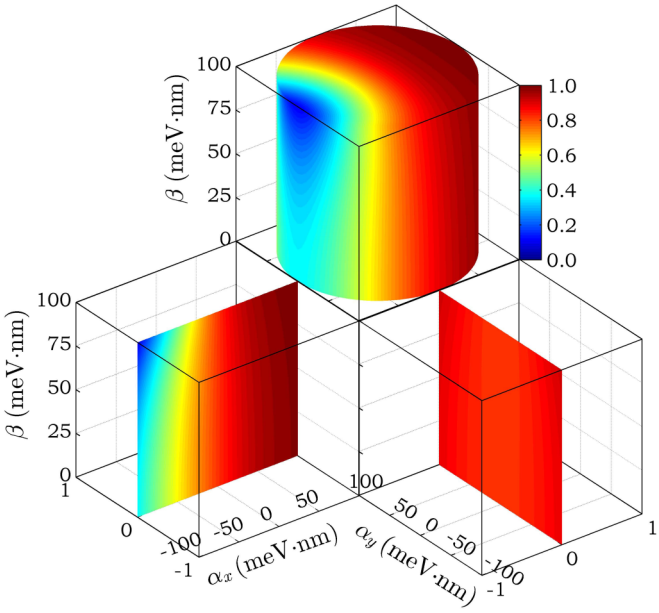

FIG. 3. The conductance isosurface plots of a 1-nm-thick domain wall in a (Ga,Mn)As nanowire with spin splitting energy $\Delta_{ex} = 0.5$ eV and Fermi energy $\epsilon_F = 0.2$ eV as a function of the Rashba spin-orbit coupling parameter in the complex plane $\alpha_R e^{i\varphi_R}$ and Dresselhaus spin-orbit coupling strength β.

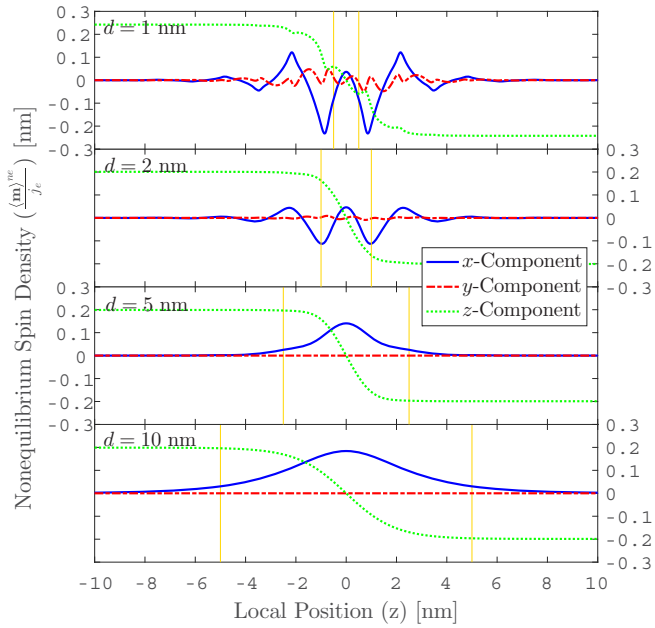

FIG. 4. The normalized nonequilibrium spin densities calculated for a wall pinned at a nanoconstriction in a p-type semiconducting ferromagnetic nanowire with the Fermi energy $\epsilon_F = 0.2$ eV and the spin splitting energy $\Delta_{ex} = 0.5$ eV, without considering the spin-orbit couplings. Calculations have been performed for different wall widths, i.e., $d = 1$, 2, 5, and 10 nm.

relative to the parameter α_x (α_y) can be clearly seen also in the presence of the Dresselhaus spin-orbit interaction. The domain wall conductance increases with the increase of the Rashba parameter $|\alpha_y|$, while it decreases (increases) by α_x for $\alpha_x < 0$ ($\alpha_x > 0$). Similarly, the Dresselhaus spin-orbit interaction has negative (positive) effect on the conductance of the domain wall for negative (positive) values of α_x. Positive values of α_x cause less growth of the domain wall conductance, whereas negative values of α_x are found to be more effective in reduction of the conductance.

It is well-known that the scattering of the carriers by geometrical domain wall potential leads to the nonequilibrium spin density within the wall and its surroundings. The local spin density normalized to the current density can be obtained using Eqs. (20) and (25). In accordance with the conventional definition of the differential magnetic moment, $\boldsymbol{\mu} = \frac{1}{2}\boldsymbol{r} \times \boldsymbol{j}$, the local spin density per unit current density could be expressed in units of length, which is depicted in Fig. 4 for different widths of the domain wall without the inclusion of spin-orbit coupling. For a 1-nm-thick domain wall, some dips (peaks) appear in the longitudinal spin density, $\langle m_z \rangle^{ne}$, that resulted from quantum interference between injected carriers and those reflected off of the wall barrier with a set of interfering points with a period of $2\pi/k^{\uparrow}$. As can be seen, they disappear when the domain wall width scales up. For wide domain walls, where the adiabatic transport is dominant, carriers spin follows the local magnetization profile. It is noted that the y component of the transverse spin density $\langle m_y \rangle^{ne}$ is always zero, unless the domain wall width scales down to 2 nm and below, where the adiabaticity does not take place and hence the precession of the electron spin about the local magnetization generates the out-of-plane component of spin density. Simultaneously, the spin density component $\langle m_x \rangle^{ne}$ oscillates symmetrically along the domain wall with a period of $2\pi/k^{\uparrow}$ and decays far outside the domain wall.

Now, I discuss the effect of the nonequilibrium spin density on the spin torque, which translates the magnetic texture, without considering the spin-orbit coupling. The calculated spin-transfer torques have been shown in Fig. 5 for a Néel-type domain wall with different widths of 1, 2, 5, and 10 nm. Calculation based on the ballistic transport of the carriers indicate that oscillatory spin-transfer torque may appear in a system with an atomic-scale domain wall, as a consequence of the nonadiabatic coupling between the carriers spin and the local magnetization. As can be seen, the nonadiabatic (out-of-plane) spin-transfer torque dramatically increases when the domain wall width scales down to the atomic dimensions which realized at the nanoconstrictions and nanocontacts. Furthermore, the adiabatic (in-plane) spin-transfer torques as well as the nonadiabatic one do not depend anymore on the magnetization gradient for such atomic-scale domain walls. In the opposite limit, when the adiabatic condition is completely fulfilled, the out-of-plane torque vanishes and the in-plane components follow the adiabatic form that is proportional to $-(\boldsymbol{j} \cdot \nabla)\boldsymbol{u}_M(r)$, as expected.

When a spin current is driven between two ferromagnetic leads with opposite magnetization directions, a nonequilibrium spin density is created in the domain wall which tends to decay in the leads away from the wall interfaces. However, the nonequilibrium spin density may be induced in the ferromagnetic leads as well as the nonferromagnetic ones in the presence of the spin-orbit interactions [60]. The

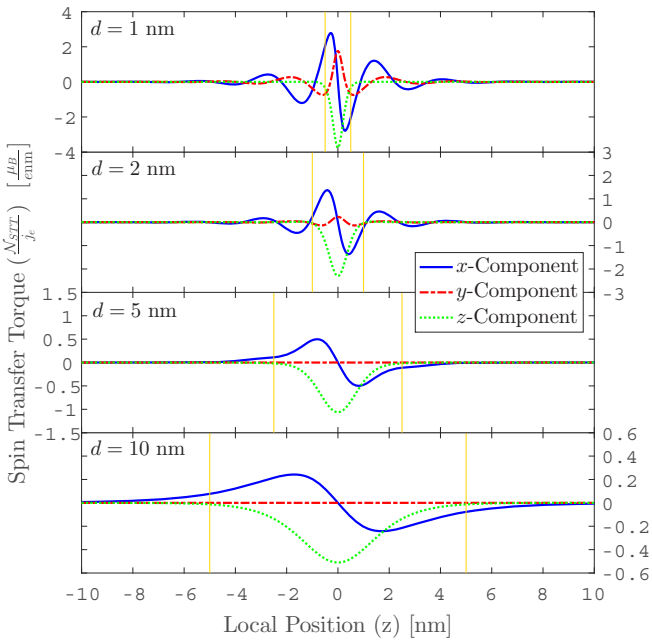

FIG. 5. The normalized spin-transfer torques calculated for a wall pinned at a nanoconstriction in a p-type semiconducting ferromagnetic nanowire. Calculations have been performed for different wall widths, i.e., $d = 1$, 2, 5, and 10 nm. Other parameters are the same as in Fig. 4.

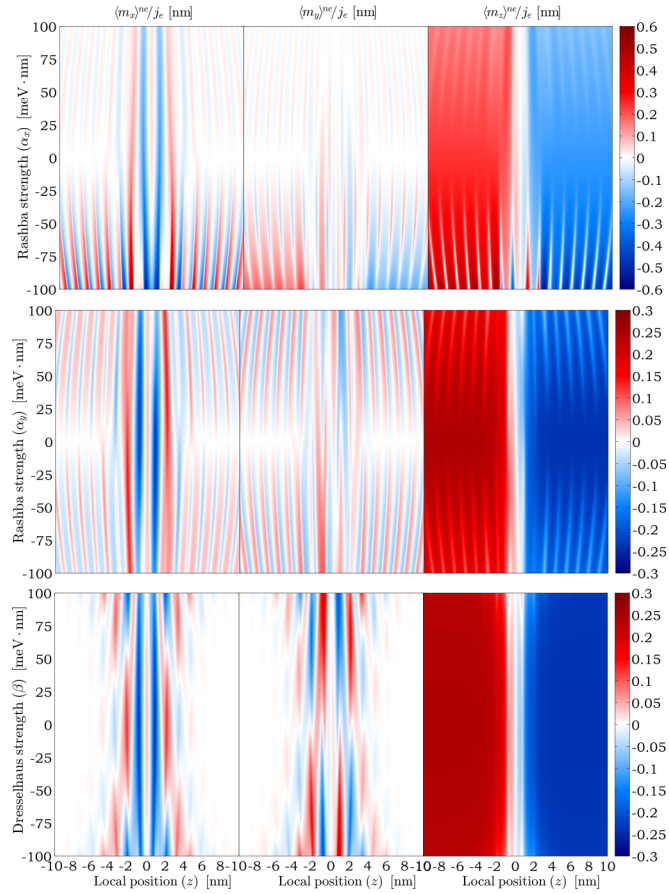

FIG. 6. Spatial distribution of the normalized in-plane ($\langle m_x\rangle^{ne}$, $\langle m_z\rangle^{ne}$) and out-of-plane ($\langle m_y\rangle^{ne}$) nonequilibrium spin density components in a p-type semiconducting ferromagnetic nanowire includes a 1-nm-thick head-to-head domain wall with Fermi energy $\epsilon_F = 0.2$ eV and spin splitting energy $\Delta_{ex} = 0.5$ eV, in the presence of the Rashba spin-orbit interaction with the effective magnetic field directed along the x axis (top), the y axis (middle), and in the presence of the Dresselhaus spin-orbit coupling with the effective field along the z axis (bottom).

nonequilibrium spin densities in a ferromagnetic nanowire including a 1-nm-thick domain wall with the Fermi energy $\epsilon_F = 0.2$ eV and the spin splitting energy $\Delta_{ex} = 0.5$ eV have been shown as contour plots in Fig. 6, where normalized with respect to the current density for different types of spin-orbit interactions, including the Rashba coupling with the effective magnetic field directed along the x axis (top panel), the y axis (middle panel), and the Dresselhaus coupling with the effective field along the z axis (bottom panel). As can be seen, the nonequilibrium spin density is not only induced within the domain wall, but also it extends to the leads, due to the coupling between the carriers spin and the momentum dependent effective field induced by the spin-orbit interactions. All components of the spin density oscillate with a period $\frac{2\pi}{\sqrt{k_F^2+2k_R^2+\sqrt{(k_F^2+2k_R^2)^2+k_{ex}^4-k_F^4}}}$ within the leads, when the Dresselhaus coupling is absent. The strength of the oscillations strongly depends on the direction of Rashba interaction. For example, the strength of the oscillations in the out-of-plane spin density, $\langle m_y\rangle^{ne}$, increases by the negative α_x, while it decreases when the direction of Rashba interaction is reversed, i.e., with increasing positive values of α_x. This is in agreement with the corresponding conductance behavior, in which the decrease in conductance for negative α_x represents the increase of the nonadiabaticity and vice versa. On the other hand, the nonadiabaticity increases with $|\alpha_y|$, regardless of its sign. In addition, the behavior of the spin densities relative to the positive values of α_y is similar to that with respect to the negative ones, but spatially reversed. In other words, the local distribution of the spin densities has inversion symmetry relative to the wall center. In the presence of the Dresselhaus spin-orbit interaction without considering the Rashba coupling, the spin density oscillations are superpositions of incoming and reflected waves with periods $\frac{2\pi}{k_D+\sqrt{k_D^2+k_F^2+k_{ex}^2}}$ and $\frac{2\pi}{-k_D+\sqrt{k_D^2+k_F^2+k_{ex}^2}}$, respectively [61]. So, the asymmetric behavior of the spin densities relative to the Dresselhaus parameter β can be understood.

A similar discussion can also be applied to the spin-orbit torque components as depicted in Fig. 7. The Rashba coupling parameter α_x with negative sign has a large effect on the spin torque, while the positive values of α_x are not so effective in enhancing the spin-torque components. Also, this coupling parameter produces an oscillatory out-of-plane torque at the leads that may change the magnetic texture of the leads. The Rashba coupling parameter α_y with inversion symmetry can increase the spin torque, too. The Dresselhaus coupling does not considerably alter the z component of the spin torque, while the other two components are effectively changed when the Dresselhaus spin-orbit interaction is taken into account.

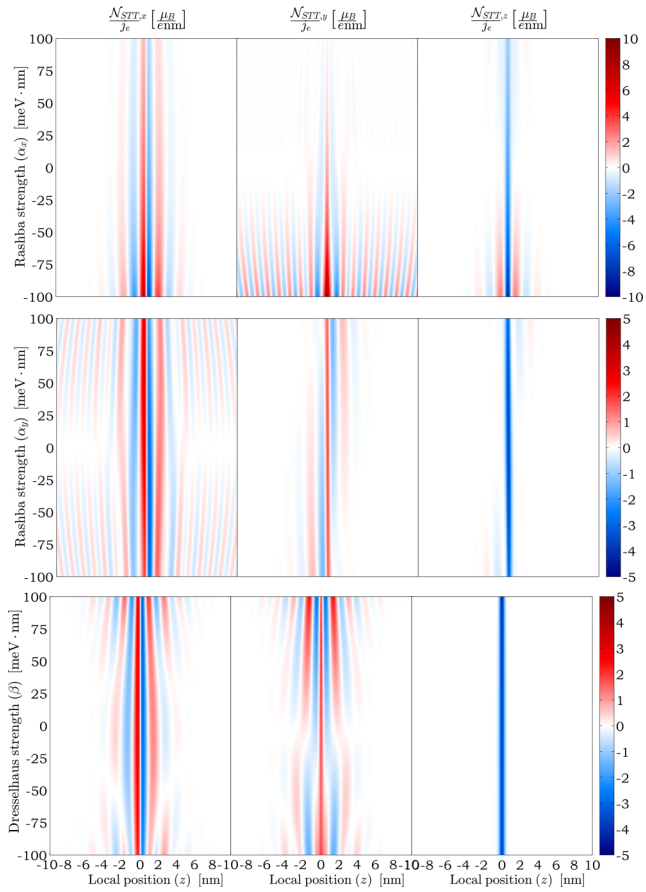

FIG. 7. Spatial distribution of the normalized in-plane ($\mathcal{N}_{\mathrm{STT},x}$, $\mathcal{N}_{\mathrm{STT},z}$) and out-of-plane ($\mathcal{N}_{\mathrm{STT},y}$) spin-transfer torque components in the presence of the Rashba spin-orbit interaction with the effective magnetic field directed along the x axis (top), the y axis (middle), and in the presence of the Dresselhaus coupling with the effective field directed along the z axis (bottom). Parameters are the same as in Fig. 6.

IV. CONCLUSION

In summary, I have investigated the influence of the D'yakonov-Perel' mechanism on the ballistic domain wall conductance, the induced nonequilibrium spin density, and the spin-transfer torque at the wall and its surroundings. The calculations have been performed for a narrow domain wall residing in a p-type spin-polarized semiconducting ferromagnetic (Ga,Mn)As nanowire with a nanoconstriction. I have utilized a helpful algorithm to solve the boundary value problem for a system of coupled differential equations arising from the Schrödinger equation with the spin-dependent potential in the magnetic wall, considering spin-orbit interactions. The transport properties of the carriers have been studied by calculating the ballistic conductance via the Landauer-Büttiker formula for a 1-nm-thick domain wall. It has been shown that the domain wall conductance increases (decreases) with the Fermi energy for positive (negative) values of α_x, while a symmetric increase is observed in the wall conductance, relative to the Rashba coupling parameter $|\alpha_y|$, which is due to the transverse electric field $-\partial_y V_\perp$ along the y axis. Similar features have also been revealed in the presence of the Dresselhaus spin-orbit interaction. Additionally, it has been found that the Dresselhaus spin-orbit coupling has negative (positive) effect on the conductance of the domain wall for negative (positive) values of α_x.

The effect of the domain wall width on the nonequilibrium spin density and the spin-transfer torque has also been explored, without considering spin-orbit couplings. It has been revealed that the out-of-plane component of the spin density $\langle m_y \rangle^{ne}$ is always zero, unless the domain wall width scales down to 2 nm and below. For such an atomic-scale domain wall, the in-plane torques as well as the out-of-plane one do not depend anymore on the magnetization gradient. Specifically, the spin-transfer torque components have been observed to become oscillatory in the leads far from the nanoconstriction, when the spin-orbit couplings are included. It has been found that the spin density and spin torque strongly depend on the sign of the spin-orbit parameters. The Rashba coupling parameter α_x with negative sign has been shown to have a large effect on the spin torque, while the positive values of α_x do not effectively change the spin-torque components. Also, the spin torque effect has been enhanced by the Rashba coupling parameter α_y, regardless of its sign. It has been demonstrated that the Dresselhaus coupling does not considerably alter the z component of the spin torque, while the other two components have been effectively changed by the Dresselhaus spin-orbit interaction.

ACKNOWLEDGMENT

This work was supported by a research grant from the University of Bonab [96/D/PA/2902].

[1] P. Xu, K. Xia, C. Gu, L. Tang, H. Yang, and J. Li, Nat. Nanotechnol. **3**, 97 (2008).
[2] M. Hayashi, L. Thomas, R. Moriya, C. Rettner, and S. S. Parkin, Science **320**, 209 (2008).
[3] W. Zhao, D. Ravelosona, J. Klein, and C. Chappert, IEEE Trans. Magn. **47**, 2966 (2011).
[4] S. S. P. Parkin, M. Hayashi, and L. Thomas, Science **320**, 190 (2008).
[5] C. Chappert, A. Fert, and F. N. Van Dau, Nat. Mater. **6**, 813 (2007).
[6] S. Fukami, T. Suzuki, K. Nagahara, N. Ohshima, Y. Ozaki, S. Saito, R. Nebashi, N. Sakimura, H. Honjo, K. Mori *et al.*, in *VLSI Technology, 2009 Symposium on* (IEEE, 2009), pp. 230–231.
[7] J. C. Slonczewski, J. Magn. Magn. Mater. **159**, L1 (1996).
[8] L. Berger, Phys. Rev. B **54**, 9353 (1996).
[9] G. Tatara and H. Kohno, Phys. Rev. Lett. **92**, 086601 (2004).
[10] C. Wang and K. Xia, Nano-Micro Lett. **1**, 34 (2009).
[11] M. Viret, D. Vignoles, D. Cole, J. M. D. Coey, W. Allen, D. S. Daniel, and J. F. Gregg, Phys. Rev. B **53**, 8464 (1996).

[12] S. Zhang, P. M. Levy, and A. Fert, Phys. Rev. Lett. **88**, 236601 (2002).

[13] J. Barnaś, A. Fert, M. Gmitra, I. Weymann, and V. K. Dugaev, Phys. Rev. B **72**, 024426 (2005).

[14] V. Fallahi and M. Ghanaatshoar, Phys. Rev. B **82**, 035210 (2010).

[15] P. B. He, X. C. Xie, and W. M. Liu, Phys. Rev. B **72**, 172411 (2005).

[16] E. Martinez, L. Lopez-Diaz, O. Alejos, and L. Torres, Phys. Rev. B **77**, 144417 (2008).

[17] J. I. Pascual, J. Méndez, J. Gómez-Herrero, A. M. Baró, N. García, and V. T. Binh, Phys. Rev. Lett. **71**, 1852 (1993).

[18] L. Olesen, E. Laegsgaard, I. Stensgaard, F. Besenbacher, J. Schiøtz, P. Stoltze, K. W. Jacobsen, and J. K. Nørskov, Phys. Rev. Lett. **72**, 2251 (1994).

[19] J. M. Krans, J. M. Van Ruitenbeek, V. V. Fisun, I. K. Yanson, and L. J. De Jongh, Nature (London) **375**, 767 (1995).

[20] B. Doudin and M. Viret, J. Phys.: Condens. Matter **20**, 083201 (2008).

[21] N. García, H. Rohrer, I. G. Saveliev, and Y. W. Zhao, Phys. Rev. Lett. **85**, 3053 (2000).

[22] S. H. Chung, M. Muñoz, N. García, W. F. Egelhoff, and R. D. Gomez, Phys. Rev. Lett. **89**, 287203 (2002).

[23] W. F. Egelhoff, L. Gan, H. Ettedgui, Y. Kadmon, C. J. Powell, P. J. Chen, A. J. Shapiro, R. D. McMichael, J. J. Mallett, T. P. Moffat *et al.*, J. Appl. Phys. **95**, 7554 (2004).

[24] N. García, M. Muñoz, and Y. W. Zhao, Phys. Rev. Lett. **82**, 2923 (1999).

[25] G. Tatara and N. García, IEEE Trans. Magn. **36**, 2839 (2000).

[26] H. Imamura, N. Kobayashi, S. Takahashi, and S. Maekawa, Phys. Rev. Lett. **84**, 1003 (2000).

[27] C. Rüster, T. Borzenko, C. Gould, G. Schmidt, L. W. Molenkamp, X. Liu, T. J. Wojtowicz, J. K. Furdyna, Z. G. Yu, and M. E. Flatté, Phys. Rev. Lett. **91**, 216602 (2003).

[28] H. D. Chopra and S. Z. Hua, Phys. Rev. B **66**, 020403 (2002).

[29] S. Z. Hua and H. D. Chopra, Phys. Rev. B **67**, 060401 (2003).

[30] V. Fallahi and R. Safaei, Phys. Rev. B **94**, 064426 (2016).

[31] S. Bohlens and D. Pfannkuche, Phys. Rev. Lett. **105**, 177201 (2010).

[32] D. Ravelosona, D. Lacour, J. A. Katine, B. D. Terris, and C. Chappert, Phys. Rev. Lett. **95**, 117203 (2005).

[33] M. Feigenson, J. W. Reiner, and L. Klein, Phys. Rev. Lett. **98**, 247204 (2007).

[34] F. X. Bronold, I. Martin, A. Saxena, and D. L. Smith, Phys. Rev. B **66**, 233206 (2002).

[35] J. H. Jiang, Y. Zhou, T. Korn, C. Schüller, and M. W. Wu, Phys. Rev. B **79**, 155201 (2009).

[36] M. Wu, J. Jiang, and M. Weng, Phys. Rep. **493**, 61 (2010).

[37] A. K. Nguyen, H. J. Skadsem, and A. Brataas, Phys. Rev. Lett. **98**, 146602 (2007).

[38] Z. Yuan and P. J. Kelly, Phys. Rev. B **93**, 224415 (2016).

[39] K. Obata and G. Tatara, Phys. Rev. B **77**, 214429 (2008).

[40] A. Manchon and S. Zhang, Phys. Rev. B **79**, 094422 (2009).

[41] H. Li, X. Wang, F. Doğan, and A. Manchon, Appl. Phys. Lett. **102**, 192411 (2013).

[42] J. D. Burton, A. Kashyap, M. Y. Zhuravlev, R. Skomski, E. Y. Tsymbal, S. S. Jaswal, O. N. Mryasov, and R. W. Chantrell, Appl. Phys. Lett. **85**, 251 (2004).

[43] V. K. Dugaev, J. Berakdar, and J. Barnaś, Phys. Rev. Lett. **96**, 047208 (2006).

[44] A. Sugawara, H. Kasai, A. Tonomura, P. D. Brown, R. P. Campion, K. W. Edmonds, B. L. Gallagher, J. Zemen, and T. Jungwirth, Phys. Rev. Lett. **100**, 047202 (2008).

[45] R. Winkler, Phys. Rev. B **62**, 4245 (2000).

[46] T. Kernreiter, M. Governale, A. R. Hamilton, and U. Zülicke, Appl. Phys. Lett. **98**, 152101 (2011).

[47] C. L. Romano, S. E. Ulloa, and P. I. Tamborenea, Phys. Rev. B **71**, 035336 (2005).

[48] V. Fallahi, Phys. Rev. B **96**, 064403 (2017).

[49] E. Tsitsishvili, G. S. Lozano, and A. O. Gogolin, Phys. Rev. B **70**, 115316 (2004).

[50] B. A. Bernevig and S. C. Zhang, Phys. Rev. B **72**, 115204 (2005).

[51] A. Chernyshov, M. Overby, X. Liu, J. K. Furdyna, Y. Lyanda-Geller, and L. P. Rokhinson, Nat. Phys. **5**, 656 (2009).

[52] V. Fallahi, J. Supercond. Nov. Magn. **30**, 2597 (2017).

[53] V. M. Ramaglia, D. Bercioux, V. Cataudella, G. D. Filippis, and C. A. Perroni, J. Phys.: Condens. Matter. **16**, 9143 (2004).

[54] M. Lundstrom, *Fundamentals of Carrier Transport* (Cambridge University Press, New York, 2009).

[55] S. Datta, *Quantum Transport: Atom to Transistor* (Cambridge University Press, New York, 2005).

[56] S. D. Pollard, L. Huang, K. S. Buchanan, D. A. Arena, and Y. Zhu, Nat. Commun. **3**, 1028 (2012).

[57] M. W. J. Prins, R. Jansen, and H. van Kempen, Phys. Rev. B **53**, 8105 (1996).

[58] D. J. Hilton and C. L. Tang, Phys. Rev. Lett. **89**, 146601 (2002).

[59] V. Fallahi and M. Ghanaatshoar, Phys. Status Solidi B **249**, 1077 (2012).

[60] J. Yao and Z. Q. Yang, Phys. Rev. B **73**, 033314 (2006).

[61] M. Ghanaatshoar and V. Fallahi, Eur. Phys. J. B **80**, 401 (2011).